

The crystalline fraction of interstellar silicates in starburst galaxies

F. Kemper^{*,1,2}, A. J. Markwick¹ and Paul M. Woods¹

¹*Jodrell Bank Centre for Astrophysics, Alan Turing Building, School of Physics and Astronomy, The University of Manchester, Oxford Road, Manchester, M13 9PL, UK*

²*Academia Sinica Institute of Astronomy and Astrophysics, P.O. Box 23-141, Taipei 10617, Taiwan, R.O.C.*

10 July 2021

ABSTRACT

We present a model using the evolution of the stellar population in a starburst galaxy to predict the crystallinity of the silicates in the interstellar medium of this galaxy. We take into account dust production in stellar ejecta, and amorphisation and destruction in the interstellar medium and find that a detectable amount of crystalline silicates may be formed, particularly at high star formation rates, and in case supernovae are efficient dust producers. We discuss the effect of dust destruction and amorphisation by supernovae, and the effect of a low dust-production efficiency by supernovae, and find that when taking this into account, crystallinity in the interstellar medium becomes hard to detect. Levels of 6.5–13% crystallinity in the interstellar medium of starburst galaxies have been observed and thus we conclude that not all these crystalline silicates can be of stellar origin, and an additional source of crystalline silicates associated with the Active Galactic Nucleus must be present.

Key words: ISM: evolution – ISM: dust, extinction – galaxies: starburst

1 INTRODUCTION

Silicates are among the most commonly-found dust species in the interstellar medium (ISM) of galaxies. Their presence is established through the detection of the mid-infrared resonances due to the Si-O stretching and the O-Si-O bending mode at 9.7 and 18 μm respectively. In galaxies, these bands are seen in absorption (Gillett et al. 1975; Sturm et al. 2000), as well as in emission (Siebenmorgen et al. 2005; Hao et al. 2005). Most of these silicates show the broad resonances characteristic of amorphous silicates, i.e., silicates showing a large degree of lattice defects, and it is generally assumed that silicates in the ISM are predominantly amorphous. In particular, the degree of crystallinity x , defined as the mass fraction of silicates that is crystalline, $x = M_X/(M_X + M_A)$, in the Galactic diffuse ISM is found to be of the order of 1% (Kemper et al. 2004, 2005). This contrasts sharply with the much higher degree of crystallinity seen in silicates in the circumstellar environments of pre- and post-main-sequence stars (see e.g. Molster & Kemper 2005, and references herein). Generally speaking, the galactic cycle of dust starts with its formation in evolved stars, followed by processing in the ISM and eventually ends with incorporation in stars and planets during

star formation. The silicates observed around Asymptotic Giant Branch (AGB) stars can have significant crystalline fractions, in particular for the high mass-loss rate OH/IR stars (up to $\sim 20\%$ Sylvester et al. 1999; Kemper et al. 2001; de Vries et al. 2010). For lower mass-loss rate AGB stars, such as Miras, the crystallinity is not well established, but is consistent with a value that does not vary with mass-loss rate (Kemper et al. 2001). For more massive stars, such as Red Supergiants (RSGs), the crystallinity of the silicates in the stellar ejecta is not well known, although isolated studies report high crystalline fractions (e.g. Molster et al. 1999), while low crystalline fractions seem to be more common (Verhoelst et al. 2009). Spoon et al. (2006) adopt a crystallinity of 15% for RSGs and Luminous Blue Variables.

In contrast to the low crystallinity in the Galactic ISM, significant amounts of crystalline silicates have been detected in the infrared spectra of Ultraluminous Infrared Galaxies (ULIRGs; Spoon et al. 2006). In a sample of 77 ULIRGs, 12 were found to show crystallinity, with crystalline-to-amorphous silicate mass ratios ranging from 0.07 to 0.15, corresponding to crystallinities of 6.5% to 13%.

The degree of crystallinity of a population of silicate grains provides a record of the processing history of those grains (see e.g. Molster & Kemper 2005). A high crystalline fraction points to a relatively high formation or processing temperature ($\sim 1000 - 1500$ K), while a large amorphous

* E-mail: ciskakemper@fastmail.net

fraction indicates that the population of grains has undergone the damaging effects of cosmic ray hits (Bringa et al. 2007), grain-grain collisions or atomic impacts in shocks (Demyk et al. 2001; Brucato et al. 2003; Jäger et al. 2003); or that it is formed at lower temperatures. Crystalline silicates may thus form in dense circumstellar environments, where the vicinity of the central star provides the required heating. The mass-loss processes of evolved stars subsequently spread these crystalline silicates into the ISM. The fact that the silicates in the ISM of the Milky Way are almost entirely amorphous (Kemper et al. 2004) suggests that the amorphisation processes in the ISM are more important than the injection of fresh crystalline silicates into the interstellar reservoir by evolved stars. For the Galaxy, an amorphisation time scale of 40 Myr has been derived from observations (Kemper et al. 2004, 2005), which is close to the experimental value of 70 Myr (Bringa et al. 2007).

Spoon et al. (2006) argue that in starburst galaxies ultraviolet (UV) photons from either the Active Galactic Nuclei (AGN) or massive stars are the only potential sources of UV photons to anneal or form the crystalline silicate mass observed. Crystallisation due to UV photons originating from the AGN is dismissed by Spoon et al. (2006), because of the observed lack of crystalline silicates in the inner 2 pc of NGC 1068 (Jaffe et al. 2004), and the fact that the crystalline silicates are only seen in absorption, and can therefore not be very warm. Spoon et al. (2006) hypothesise that the crystalline silicates must be produced by massive stars originating from the starburst. In this paper, we will investigate the viability of the build-up of crystalline silicates due to the starburst activity in ULIRGS as proposed by Spoon et al. (2006), and compare the crystalline fraction to the levels observed by these authors. The alternative formation of crystalline silicates due to AGN activity will be the subject of a separate future study. This future work will be based on the predicted formation of dust in the quasar wind rising from the accretion disk (Elvis et al. 2002), where conditions may be similar to those present in AGB star winds, a class of very efficient dust producers. Crystalline silicates may form in quasar winds if the conditions are right. Indeed, we have already observed crystalline silicates in the quasar wind of PG 2112+059 (Markwick-Kemper et al. 2007).

2 THE MODEL

2.1 Injection of mass in the ISM of starburst galaxies

When a starburst occurs, a large fraction of the gas available in molecular clouds will be triggered into forming stars.

Essentially following the method described by Tinsley (1980), we assume that the burst of star formation occurs at a constant rate $\psi(t) = \psi_0$ for $t_0 < t < t_1$, and that the star formation rate before t_0 and after t_1 is negligible. The distribution of stars over the mass spectrum follows the initial mass function (IMF) $\phi(m) = N_0 m^{-(1+a)}$. We adopt the IMF as described by Kroupa (2001), who derive a value of $a = 1.3$ for $M > 1 M_\odot$, which is not too dissimilar from the original Salpeter IMF ($a = 1.35$ for the entire mass range; Salpeter 1955). About 51% of the mass in a star formation event is contained in the stars more massive than the Sun (Kroupa 2001), from which we can calculate N_0 by solving

$$\int_{m=1}^{\infty} \phi(m) dm = N_0 \int_1^{\infty} m^{-(1+a)} dm = 0.51. \quad (1)$$

We find that $N_0 = 0.663$ satisfies this equation. Since the duration of the starburst will be much shorter than the life time of the Sun (τ_\odot), we do not need to consider mass-loss for low mass stars, so the exact shape of the ISM below $M < 1 M_\odot$ is irrelevant. Naturally, setting the upper integration boundary to $m = \infty$ results in unrealistically high stellar masses, but since the IMF is a very steep power-law, the numerical contribution from hypothetical stars with $M > 120 M_\odot$ is negligible.

The time that a star spends on the Main Sequence is approximated by $\tau_{\text{MS}} \propto \frac{M}{L}$, while the mass-luminosity relation states that $L \propto M^\eta$, with $\eta \approx 3.35$ for stars with $1 M_\odot < M < 40 M_\odot$ (e.g. Kippenhahn & Weigert 1990). Thus we find for the lifetime of a star on the Main Sequence – using solar units, e.g. $m(M_\odot)$ and $t(\tau_\odot)$ – that $\tau_m = m^{1-\eta}$.

It is possible to set up an equation for the ejection rate $E(t)$ at which gas is being expelled from a population of stars formed during a starburst in a galaxy (Tinsley 1980). Assuming the mass-loss occurs instantaneously after a lifetime τ_m on the Main Sequence, a star formed at time $(t - \tau_m)$ ejects its shell at time t . In order to obtain the ejection rate, one needs to integrate over all masses m larger than m_t , the stellar mass corresponding to lifetime $\tau_m = t$. Thus, the ejection rate is

$$E(t) = \int_{m_t}^{\infty} (m - w_m) \psi(t - \tau_m) \phi(m) dm \quad (2)$$

where w_m is the mass of the remnant after the mass loss. By substituting $\tau_m = m^{1-\eta}$ and $m_t = t^{\frac{1}{1-\eta}}$ and using the initial mass function and our assumption that the star formation rate is constant at a value of ψ_0 during the burst, the ejection rate $E(t)$ can be written as

$$E(t) = \int_{m=t^{\frac{1}{1-\eta}}}^{\infty} (m - w_m) \psi_0 N_0 m^{-(1+a)} dm. \quad (3)$$

2.2 The remnant mass function

We adopt the strategy utilised by Dabringhausen et al. (2009) to describe the remnant mass function, w_m . It slices the stars with $m \geq 1$ into three categories: those that leave white dwarfs ($m < 8$), those that leave neutron stars ($8 \leq m < 25$) and those that leave black holes ($m \geq 25$) as their stellar remnants. Dabringhausen et al. (2009) arrive at the following expressions for the remnant mass of the form $w_m = f_w m + w_{m_0}$, with f_w and w_{m_0} determined in each category to be:

$$w_m = \begin{cases} 0.109 m + 0.394 & \text{for } 1 \leq m < 8 \\ 1.35 & \text{for } 8 \leq m < 25 \\ 0.1 m & \text{for } 25 \leq m \end{cases} \quad (4)$$

2.3 A starburst of finite duration

In order to calculate the ejection rate, we can distinguish two different eras: during the starburst ($0 < t < \sigma$) and af-

ter the starburst ($t > \sigma$). Within each era, we can subdivide into three different regimes, corresponding to the lifetimes of the stellar mass ranges described by Dabringhausen et al. (2009), defined by the boundaries $\tau_8 = 8^{1-\eta}\tau_\odot = 7.5 \cdot 10^{-3}\tau_\odot$ and $\tau_{25} = 25^{1-\eta}\tau_\odot = 5.2 \cdot 10^{-4}\tau_\odot$. We assume that $\sigma > \tau_8$.

2.3.1 During the starburst: $0 < t < \sigma$

- Phase I: $t < \tau_{25}$:

Only the most massive stars ($m > 25$) have started losing mass, and for these objects the remnant mass is given by $w_m = 0.1m$ (Eq. 4), and thus Eq. 3 becomes

$$E(t) = \int_{m=m_t}^{\infty} m(1-f_w)\psi_0 N_0 m^{-(1+a)} dm \quad (5)$$

which simplifies to

$$E(t) = -\psi_0 N_0 (1-f_w) \left(\frac{1}{1-a} m_t^{1-a} \right) \quad (6)$$

with $N_0 = 0.663$ and $f_w = 0.1$, and $m_t = (t/\tau_\odot)^{1/1-\eta}$.

- Phase II: $\tau_{25} < t < \tau_8$:

During this phase, two components contribute to the ejection rate: $E(t) = E_1 + E_2(t)$, with E_1 a constant value due to the ejection rate by the most massive stars ($m > 25$), and $E_2(t)$ an increasing component due to the ejection by intermediate mass stars ($8 < m < 25$). To obtain E_1 , we integrate Eq. 5 between $m = 25$ and ∞ , and find that

$$E_1 = -(1-f_w)\psi_0 N_0 \frac{1}{1-a} 25^{1-a} \quad (7)$$

which, for $f_w = 0.1$, $N_0 = 0.663$, and $a = 1.3$ results in $E_1 = 0.76\psi_0$.

To obtain $E_2(t)$, we integrate

$$E_2(t) = \int_{m=m_t}^{25} (m-w_m)\psi_0 N_0 m^{-(1+a)} dm \quad (8)$$

and find

$$E_2(t) = \psi_0 N_0 \left(25^{-a} \left(\frac{25}{1-a} + \frac{w_m}{a} \right) - m_t^{-a} \left(\frac{m_t}{1-a} + \frac{w_m}{a} \right) \right) \quad (9)$$

with $w_m = 1.35$.

- Phase III: $\tau_8 < t < \sigma$, with $\sigma < \tau_\odot$:

During this phase, the ejection rate can be written as $E(t) = E_1 + E_2 + E_3(t)$ with, E_1 given by Eq. 7, and E_2 obtained by substituting $m_t = 8$ into Eq. 8. This yields

$$E_2 = \psi_0 N_0 \left(25^{-a} \left(\frac{25}{1-a} + \frac{w_m}{a} \right) - 8^{-a} \left(\frac{8}{1-a} + \frac{w_m}{a} \right) \right) \quad (10)$$

which, for $w_m = 1.35$ gives $E_2 = 0.47\psi_0$.

The ejection rate by low mass stars ($m < 8$) $E_3(t)$ can be obtained from Eq. 3:

$$E_3(t) = \int_{m=m_t=(t/\tau_\odot)^{\frac{1}{1-\eta}}}^8 (m-w_m)\psi_0 N_0 m^{-(1+a)} dm \quad (11)$$

with $w_m = f_w m + w_{m_0}$. This can be rewritten as

$$E_3(t) = \psi_0 N_0 \left[8^{1-a} \left(\frac{1-f_w}{1-a} + \frac{w_{m_0}}{a} \cdot \frac{1}{8} \right) - m_t^{1-a} \left(\frac{1-f_w}{1-a} + \frac{w_{m_0}}{a} \cdot \frac{1}{m_t} \right) \right] \quad (12)$$

2.3.2 After the starburst: $t > \sigma$

When a starburst of duration σ has stopped, there are no longer any stars with $m > ((t-\sigma)/\tau_\odot)^{\frac{1}{1-\eta}}$ in the galaxy, thus constraining the upper limit of the integration to obtain the ejection rate.

- Phase IV: $t - \sigma < \tau_{25}$:

Shortly after the starburst has stopped stars with $m > 25$ still exist, and we can write for the ejection rate: $E(t) = E'_1(t) + E_2 + E_3(t)$. E_2 and $E_3(t)$ are given by Eqs. 10 and 12. For $E'_1(t)$ we can write, with $m_{t-\sigma} = ((t-\sigma)/\tau_\odot)^{1/1-\eta}$,

$$E'_1(t) = \int_{m=25}^{m_{t-\sigma}} m(1-f_w)\psi_0 N_0 m^{-(1+a)} dm \quad (13)$$

which we can rewrite as:

$$E(t) = \psi_0 N_0 (1-f_w) \left[\frac{1}{1-a} \left\{ m_{t-\sigma}^{1-a} - 25^{1-a} \right\} \right] \quad (14)$$

- Phase V: $\tau_{25} < t - \sigma < \tau_8$.

In this phase, high-mass stars ($m > 25$) are extinct and no longer contribute to the ejection rate, which has now become $E(t) = E'_2(t) + E_3(t)$, with $E_3(t)$ again equal to the result of Eq. 12. For $E'_2(t)$ we can write

$$\begin{aligned} E'_2(t) &= \int_{m=8}^{m_{t-\sigma}} (m-w_m)\psi_0 N_0 m^{-(1+a)} dm \\ &= \psi_0 N_0 \left[m_{t-\sigma}^{-a} \left(\frac{m_{t-\sigma}}{1-a} + \frac{w_m}{a} \right) - 8^{-a} \left(\frac{8}{1-a} + \frac{w_m}{a} \right) \right] \end{aligned} \quad (15)$$

with $m_{t-\sigma} = ((t-\sigma)/\tau_\odot)^{1/1-\eta}$.

- Phase VI: $t - \sigma > \tau_8$

At this late time after the starburst only low-mass stars with $m < 8$ are still in existence, and thus

$$\begin{aligned} E(t) &= E'_3(t) \\ &= \psi_0 N_0 \left[m_{t-\sigma}^{1-a} \left(\frac{1-f_w}{1-a} + \frac{w_{m_0}}{a} \cdot \frac{1}{m_{t-\sigma}} \right) - m_t^{1-a} \left(\frac{1-f_w}{1-a} + \frac{w_{m_0}}{a} \cdot \frac{1}{m_t} \right) \right] \end{aligned} \quad (16)$$

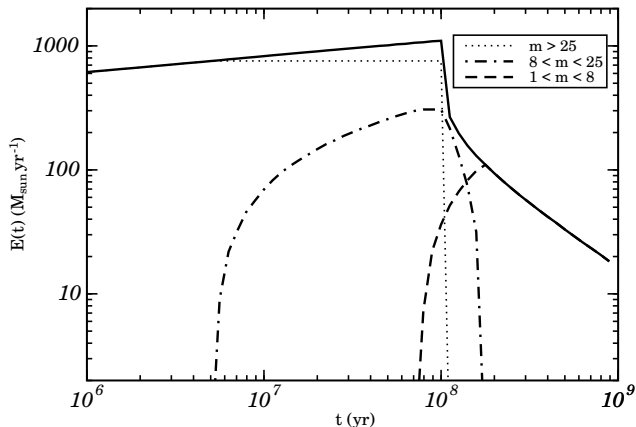


Figure 1. Stellar mass ejection rate into the ISM of a starburst galaxy with a star formation rate $\psi = 1000 M_{\odot} \text{ yr}^{-1}$, as a function of time after the beginning of the starburst (solid line). The duration of the starburst is 100 Myr. The dotted, dash-dotted and dashed lines indicate the contributions by high, intermediate and low mass stars respectively.

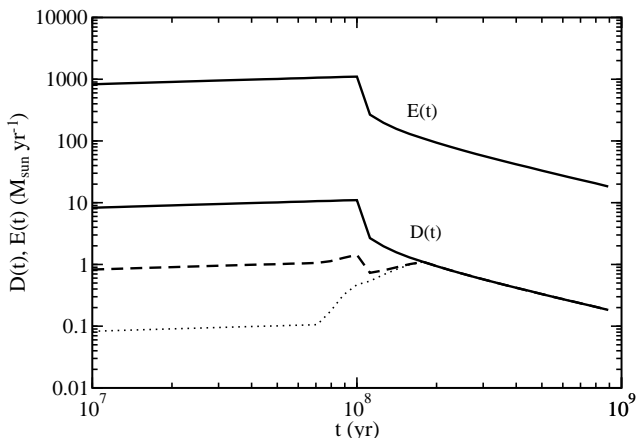


Figure 2. Dust production rate $D(t)$ in a starburst galaxy, compared to the stellar mass ejection rate $E(t)$, both indicated by solid lines. The dust-to-gas ratio d is assumed to be 0.01 in all ejecta. The dashed and dotted lines show the dust production rates in cases where supernovae produce dust at 10 or 100 times lower efficiencies, respectively.

2.4 Mass ejection rates and dust production

In Fig. 1 the resulting ejection rate $E(t)$ throughout phases I–VI is shown for a starburst of $1000 M_{\odot} \text{ yr}^{-1}$ and a duration of 100 Myr, as well as the ejection by high, intermediate and low mass stars specifically. It is clear that during the burst of star formation supernovae ejecta from the most massive stars ($m > 25$) dominate the mass return to the ISM, but that after the starburst has ended, intermediate- and low-mass stars are important.

For each of the regimes, the dust production rate $D(t)$ is related to the mass ejection rate by $D(t) = E(t)d$, in which d is the dust-to-gas ratio. In the simplest scenario we assume that low, intermediate and high mass stars are all equally efficient dust producers, for which we use the commonly-used value of $d = 0.01$. This gives rise to the solid line labelled $D(t)$ in Fig. 2. The dust-production efficiency of supernovae

is a hot topic in research because of its implications for the presence of dust at high redshift, and the consensus seems to be that dust production in supernova ejecta is not as efficient as in the outflows of lower mass stars (e.g. Sugerman et al. 2006; Fox et al. 2010). We have thus also considered values of 0.001 and 0.0001 for d , for the ejecta of high and intermediate mass stars ($m > 8$), all of which produce supernovae. The resulting $D(t)$ is shown in Fig. 2, by the dashed and dotted lines respectively.

2.5 The dust budget in the ISM of a galaxy

In our model, we will consider two separate dust reservoirs to be present in a galaxy: a crystalline silicate reservoir with a mass M_X and an amorphous silicate reservoir with a mass M_A . The injection of new silicate material $D(t)$, as described in Sect. 2.4, affects both reservoirs, although not in equal amounts. We use x_* to denote the fraction of silicate mass in crystalline form produced by stars. Another possible source of silicates is dust formation in the ISM itself, which can be generally expressed as $F_A(t)$ and $F_X(t)$ for amorphous and crystalline silicates respectively.

We include the transitions between both reservoirs due to annealing or destruction of the lattice structure, which occur at a rate k_1 for the amorphisation of crystalline material and k_2 for the crystallisation of amorphous silicates.

Finally, the processes that remove material from both dust reservoirs include grain destruction by supernova shocks and cosmic ray hits, but also astration and incorporation in planet-forming disks. We summarise these terms as dust destruction, occurring at rates of k_3 and k_4 for crystalline and amorphous silicates respectively.

Following Eq. 5 from Kemper et al. (2004), these rates can be written as a set of coupled differential equations:

$$\begin{cases} \frac{dM_X}{dt} = x_*D(t) - k_1M_X + k_2M_A - k_3M_X + F_X(t) \\ \frac{dM_A}{dt} = (1 - x_*)D(t) + k_1M_X - k_2M_A - k_4M_A + F_A(t). \end{cases} \quad (17)$$

In interstellar conditions, the crystallisation rate k_2 will be negligible, as annealing requires the grains to be heated to $\gtrsim 1000$ K, which is unlikely to occur. We also assume that the destruction rates for both types of silicates are equal: $k_3 = k_4 = 2 \times 10^{-9} \text{ yr}^{-1}$ (Kemper et al. 2004), and that dust formation in the ISM can be ignored: $F_X(t) = F_A(t) = 0$. For the amorphisation rate of crystalline silicates we take the rate $k_1 = 2.5 \times 10^{-8} \text{ yr}^{-1}$, in accordance with Kemper et al. (2005).

Eq. 17 allows us to investigate the time dependence of the crystalline and amorphous silicate masses, and compare the results with the observational constraints (Spoon et al. 2006). Instantaneous mixing of the silicates is assumed.

2.6 Fitting parameters

The values for the fixed parameters and the fitting ranges for the free parameters required to reproduce the observed crystallinities are set as follows. The star formation rate ψ_0 is allowed to vary between 10 – $1000 M_{\odot} \text{ yr}^{-1}$. The total initial dust mass in a galaxy is varied between 10^7 – $10^8 M_{\odot}$, with an initial crystalline fraction $x_{\text{ISM}} \leq 0.01$. It should be

noted that both the initial dust mass and the star formation rate are related to the gas mass in the galaxy, and both will go up for a larger gas reservoir. The crystallinity in the stellar ejecta x_* is taken to be 0.10–0.20. The duration of the starburst is allowed to run until $0.01 \tau_\odot$, or 100 Myr, which is well beyond the commonly accepted value of 5–10 Myr for the duration of starburst, although recent work on dwarf galaxies suggest that starburst may last a few 100 Myr (McQuinn et al. 2010).

3 RESULTS

We have numerically evolved the system using Eq. 17. The results of a run with an initial dust mass $M_X + M_A = 10^8 M_\odot$, star formation rate $\psi_0 = 1000 M_\odot \text{ yr}^{-1}$ and crystallinity $x_* = 0.2$ for the silicates in the stellar ejecta in Fig. 3. In this case supernovae are considered equally efficient dust producers as low mass stars, with $d = 0.01$ over the entire stellar mass range. Panel **a)** shows the silicate ejection rate throughout time for a starburst of $0.01 \tau_\odot$ in duration. Due to the contribution of these ejecta, the total silicate mass $M_X + M_A$ in the galaxy increases (panel **b)**), and levels off after the end of the starburst (dashed line). The dash-triple-dotted line indicates the destruction time scale of 400 Myr, which is due to rates k_3 and k_4 . At this point the total dust mass has decreased significantly from its peak during the starburst. The mass M_X contained in crystalline silicates (panel **c)**) closely follows the ejection rate, since the amorphisation time scale is short (40 Myr, based on k_1 , indicated with a dotted line). The crystallinity in the ISM $x_{\text{ISM}} = M_X / (M_X + M_A)$ (Kemper et al. 2004) is plotted in panel **d)** and appears to peak before the amorphisation time scale has elapsed, at around 20 Myr. A significant level of crystallinity may build up for a brief period of time. In this particular example, we find levels of $x_{\text{ISM}} \approx 10 - 11\%$.

The definition of crystallinity used here is based on the work presented in an earlier paper (Kemper et al. 2004), and differs from the crystalline-to-amorphous ratio $N_{\text{cr}}/N_{\text{am}}$ measured by Spoon et al. (2006). Their ratios of 0.07–0.15 therefore translate to crystallinities x_{ISM} of 6.5% – 13% for the interstellar silicates in these ULIRGs, experiencing starbursts. The peak crystallinity in our calculation of $\sim 10 - 11\%$ falls within this range.

However, a star formation rate of $\psi_0 = 1000 M_\odot \text{ yr}^{-1}$ is on the high end of the range seen in starburst galaxies (e.g. Weedman & Houck 2008), and values of 10–100 seem to be more common (e.g. Kennicutt 1998). When these lower values are used in the model calculations, the crystallinity of the silicates in the ISM builds up more slowly (Fig. 4), and peaks at values below the measurements by Spoon et al. (2006).

3.1 The effect of supernovae

As Figs. 3 and 4 demonstrate, the levels of crystallinity reached in starburst galaxies with high ($1000 M_\odot \text{ yr}^{-1}$; Fig. 3) and intermediate ($> 100 M_\odot \text{ yr}^{-1}$; Fig. 4) star formation rates are in line with the range of $x = 6.5 - 13\%$ that is observed by Spoon et al. (2006). However, these calculations were performed under the assumption that the

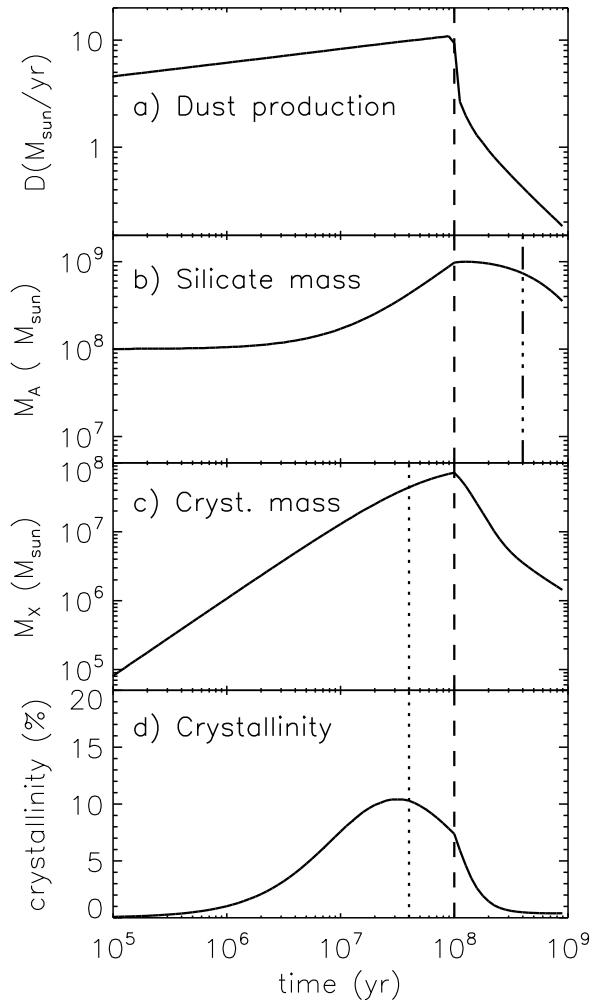


Figure 3. Results from model calculations, with the initial interstellar silicate mass $M_X + M_A = 10^8 M_\odot$, the star formation rate $\psi_0 = 1000 M_\odot \text{ yr}^{-1}$, the stellar crystallinity $x_* = 0.2$ and the dust-to-gas ratio $d = 0.01$ for all stars. Panel **a)** displays the total injection rate of stellar dust into the ISM as a function of time after the beginning of the starburst. In panel **b)** the total silicate mass in the galaxy is shown. Panel **c)** shows the crystalline silicate mass in solar masses, and finally, in panel **d)** we show the crystallinity, defined as the crystalline silicate mass divided by the total silicate mass. The dashed line indicates the end of the starburst $t_1 = 10^8$ yrs. The dashed-triple-dotted and the dotted lines indicate destruction and amorphisation time scales in the ISM respectively.

dust production by supernovae is efficient, with a dust-to-gas mass ratio d in the stellar ejecta of 0.01, independent of initial stellar mass. However, when we, following work by e.g. Sugerman et al. (2006) and Fox et al. (2010) confirming that supernovae are not efficient dust producers, consider a 10 or 100 times lower dust formation efficiency in the supernovae ejecta (affecting all stars with $m > 8$) a different picture arises.

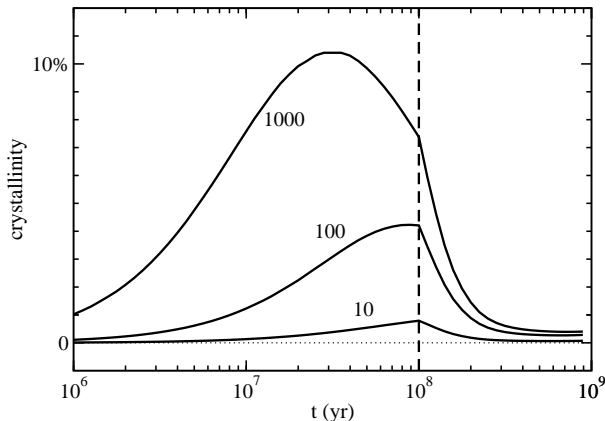


Figure 4. Crystallinity in models with star formation rates ψ_0 of 1000, 100 and $10 M_\odot \text{ yr}^{-1}$ (solid lines). The other model parameters are set as described in the beginning of Sect. 3. The dashed line indicates the end of the starburst.

The top two panels of Fig. 5 show the amorphous and crystalline silicate mass in the starburst galaxy, using values of $d = 0.01$ (solid lines), 0.001 (dashed lines) and 0.0001 (dotted lines) describing the supernova dust productivity, while the dust production efficiency of low mass stars ($m < 8$) is kept at $d = 0.01$. The two sets of lines in the top panel of Fig. 5 arise from different initial dust masses in the ISM (see caption). These plots show that the overall dust production dramatically decreases, and that the peak in dust mass shifts to a later time. The crystalline silicate mass is even 1 or 2 orders of magnitude lower during the starburst phase, and is no longer dependent on the supernova dust productivity 20 Myr after the starburst. This is due to the fact that the amorphisation time scale is very short, and all crystalline silicates present at this time are freshly produced by low mass stars.

The crystallinity x , in the bottom panel of Fig. 5 shown for $\psi_0 = 1000 M_\odot \text{ yr}^{-1}$ and an initial dust mass of $10^8 M_\odot$, evolves differently with time for different dust production efficiencies in supernova, however the width of the curve is determined by the amorphisation rate k_1 . At the lowest efficiency we considered, $d = 0.0001$ the crystalline fraction is in fact dominated by the produce of low mass stars, which peaks after the end of the starburst, in this case. The peak crystalline fraction is also considerably lower for low dust production efficiencies, and for this very high star formation rate only a level of 4% is reached, just below the lowest values of 6.5% observed by Spoon et al. (2006). After 5–10 Myr, the generally accepted value for the duration of a starburst, only small amounts of crystallinity have built up, even for the most favourable set of parameters.

4 DISCUSSION

Through constructing an ISM dust evolution model we have been able to explain the crystallinities observed by Spoon et al. (2006) in a sample of 12 ULIRGs, out of a larger set of 77 analysed. The observed crystallinities range from 6.5 to 13%. We remark, however, that the derived crystallinity is high, due to the use of the $16.5 \mu\text{m}$ forsterite feature. This is intrinsically one of the weaker forsterite

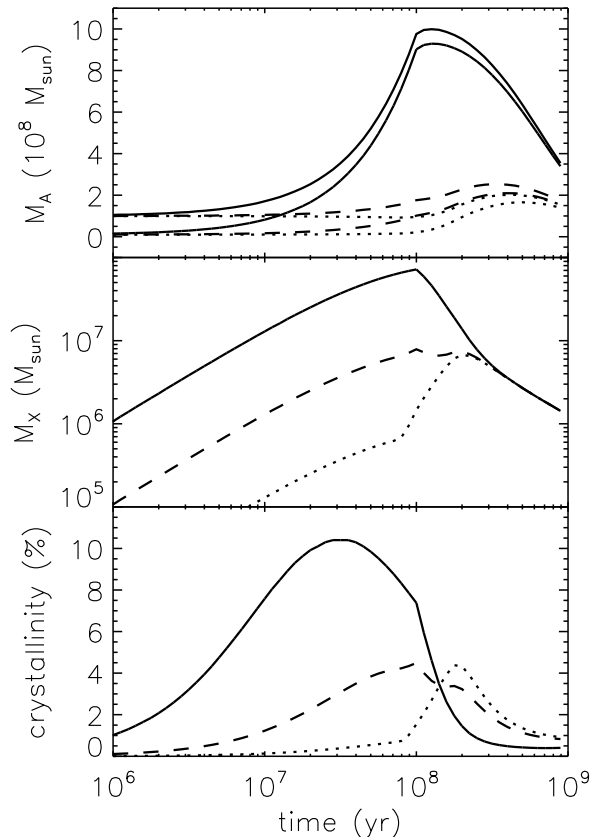


Figure 5. The amorphous and crystalline dust masses in a starburst over time, for three different SN dust production efficiencies: $d = 0.01$ (solid lines), $d = 0.001$ (dashed lines) and $d = 0.0001$ (dotted lines). The first panel shows the amorphous silicate mass M_A in the ISM of a starburst galaxy, with the two curves in each line style representing the initial ISM dust masses of $10^7 M_\odot$ (lower lines) and $10^8 M_\odot$ (upper lines). The second panel shows the crystalline silicate mass M_X , and the third panel the crystalline fraction $x = M_X / (M_X + M_A)$ of silicates in the ISM of a starburst galaxy as a function of time. For all models, ψ_0 is set to $1000 M_\odot \text{ yr}^{-1}$.

resonances (Jäger et al. 1998), and thus a large amount of forsterite is required to explain the optical depth in this feature. Spoon et al. (2006) chose this feature for their analysis because it was the only feature clearly observed in all 12 objects. Using Fig. 5 and Eq. (1) from their paper, we estimate that the crystallinity could be a factor of ~ 3 or ~ 4.5 lower, when using the 18 or $23 \mu\text{m}$ features respectively. This should, however, be compared to the lack of a crystalline silicate detection in the ISM of the Milky Way (Kemper et al. 2004). Additionally, crystallinities in the ULIRG sample can only be derived for all sources using the $16.5 \mu\text{m}$ feature, and we therefore use the results presented by Spoon et al. (2006) at face value.

Using the relatively high values of $1000 M_\odot \text{ yr}^{-1}$ for the star formation rate and a crystallinity of 20% in the stellar ejecta we achieve interstellar crystallinities of $> 10\%$, under the assumption that supernovae are efficient dust producers, with a dust-to-gas ratio $d = 0.01$ in their ejecta. As the

time-dependent plots show, detectable levels of crystallinity are only a temporary condition, which is consistent with only seeing it in part of the ULIRG sample studied, with the timing and the duration of detectable levels depending on the model parameters. In the case that supernovae are important dust producers, the crystallinity of the silicates in the ISM peaks shortly after the starburst on a time scale shorter than the amorphisation time scale of 40 Myr. For the parameters used in our fiducial model, we find that the crystallinity is highest some 10–20 Myr after the starburst and that crystalline silicates can make up $\approx 11\%$ of the silicate material.

4.1 Evaluation of the input parameters

The input parameters used are on the extreme end of the range observed, particularly for the star formation rate ψ_0 , the crystallinity x_* of the silicates in stellar ejecta and the (supernova) dust formation efficiency d . We also discuss the role of supernovae in general.

First, for more typical star formation rates of $\psi_0 = 10 - 100 M_\odot \text{ yr}^{-1}$ the interstellar crystallinity is much less enhanced during the starburst (see Fig. 4), making it harder to explain the observed values.

Second, the interstellar crystallinity scales linearly with the crystallinity of stellar ejecta used, where $x_* = 20\%$ is on the high side. More typical values are around 10% (Kemper et al. 2001), although de Vries et al. (2010) have shown that the forsterite abundance (one of the species contributing to the crystallinity) is closer to 12%. Unfortunately, the crystallinity can only be measured in stars with the densest winds (Sylvester et al. 1999); crystallinities up to about 20% in the more numerous low density winds would remain undetected (Kemper et al. 2001). Thus, 20% could be regarded as an upper limit to the crystallinity in stellar ejecta, for classes of objects where no specific measurements exist.

4.1.1 The role of supernovae

The role of supernovae in the mineralogical evolution of a galaxy remains uncertain, for a number of reasons. First, little is known about the mineralogy of supernovae ejecta. The small number of studies available (e.g. Rho et al. 2009) do not establish the crystallinity of the produced silicates. Second, the dust production efficiency d of supernovae has been shown to be low (e.g. Sugerman et al. 2006; Fox et al. 2010) compared to lower mass stars. On the other hand, studies of the Cas A and Kepler supernova remnants suggest significant amounts of dust may have formed (Morgan et al. 2003; Dunne et al. 2003), although in one of these particular studies foreground emission may have been interpreted as coming from the supernova remnant itself (Krause et al. 2004). Thus, d may range from 0.0001 to 0.01. In Fig. 5, the effect of a low dust formation efficiency in supernovae on the dust population in a galaxy shows that the crystallinity does peak at much later times and at lower values due to his effect. Indeed, at a supernova dust production rate of $d = 0.0001$, the dust production, and thus the crystallinity, is dominated by low-mass stars ($m < 8$, with $d = 0.01$), and by the time the crystallinity peaks these galaxies are no longer recognisable as starburst galaxies.

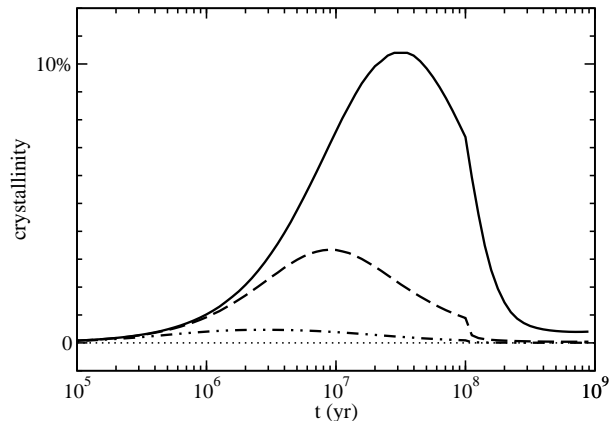


Figure 6. Crystalline fraction of silicates $x = M_X/(M_X + M_A)$ in the ISM of a starburst galaxy as a function of time, for three different amorphisation rates $k_1 = 2.5 \cdot 10^{-8}$ (solid line), $k_1 = 2.5 \cdot 10^{-7}$ (dashed line) and $k_1 = 2.5 \cdot 10^{-6} \text{ yr}^{-1}$ (dash-dotted line). The curves shown are for the initial dust mass of $10^8 M_\odot$, and a star formation rate of $1000 M_\odot \text{ yr}^{-1}$.

Third, the higher supernova rate has its effect on the amorphisation rate. The values used for k_1 are derived for Galactic conditions but these may be significantly higher in starburst galaxies due to the enhanced rate of shocks and cosmic ray hits. We have investigated the effect of an enhanced supernova rate, by increasing k_1 up to a factor of 100. Increasing these rates is detrimental to the crystalline fraction, with an increase of a factor 100 reducing the crystalline fraction in the ISM to $\ll 1\%$ (Fig. 6).

Finally, as Spoon et al. (2006) argue, supernova progenitors, such as RSGs and Luminous Blue Variables, may produce significant amount of crystalline silicates (e.g. Molster et al. 1999; Voors et al. 1999), and thus contribute to the interstellar crystallinity. However, the subsequent supernova shocks travelling through these earlier ejecta will destroy a large fraction of the grains by sputtering (Jones et al. 1994, 1996). The crystalline and amorphous silicate materials (assumed to be affected in equal amounts) will be returned to the gas phase. Thus, the ISM will be enriched by the atomic building blocks of silicates, but in gaseous form. Moreover, the high supernova rate in starburst galaxies will affect the dust destruction rates k_3 ($= k_4$), returning even more dust to the gas-phase.

4.1.2 Dust formation in the ISM

The (re-)condensation of dust from the gas phase in the ISM will also affect the crystallinity. In our model calculations, we assumed that the dust formation in the ISM itself is negligible as a source of dust, hence $F_A = F_X = 0$. However, calculations by Zhukovska et al. (2008) show that it can be the most important process that contributes to the dust content of the Milky Way. Since dust formation and dust growth at the low temperatures prevalent in molecular clouds yields only amorphous silicates, inclusion of this factor will further reduce the crystallinity of interstellar silicates.

4.2 Low crystallinities in typical starbursts

Although our models are successful in explaining the crystallinity observed in ULIRGs (Spoon et al. 2006), we find that this is only the case for an extreme set of input parameters. For more usual values for the star formation rate and the dust formation efficiency in supernovae, and when the effect of supernovae on grain destruction and amorphisation is taken into account, we find that the observed crystallinity of silicates cannot be explained by a starburst driven model only. Thus, we conclude that the high level of crystallinity derived by Spoon et al. (2006) is inconsistent with the formation of crystalline silicates in stellar ejecta only. However their observations are also consistent with crystallinities a factor of ~ 3 –4.5 lower than what is reported in their paper when different resonances are used, in which case our model calculations show that stellar sources could indeed explain the observed crystallinity, using reasonable parameters.

5 CONCLUSION

In order to explain the high crystalline fraction of silicates in ULIRGs, as reported by Spoon et al. (2006) we find that an additional source of crystalline silicates (or crystallisation of amorphous silicates) must be present, related to the AGN itself, rather than the starburst activity. In this case, the crystallisation will occur due to heating by (UV) photons from the AGN environment, rather than (massive) stars. A potential scenario may include the formation of (crystalline) silicates in quasar winds (Elvis et al. 2002). In addition, further observational studies are useful to better establish the crystalline fraction of silicates in ULIRGs, and validate the conclusions presented here.

ACKNOWLEDGEMENTS

We thank Sacha Hony and Svitlana Zhukovska for careful reading of the manuscript. Their comments and suggestions have led to a considerable improvement of this work. This research benefited from the award of a Leverhulme Research Fellowship to F. Kemper.

REFERENCES

- Bringa E. M., et al. 2007, *ApJ*, 662, 372
 Brucato J. R., Strazzulla G., Baratta G., Colangeli L., 2003, *A&A*, 413, 395
 Dabringhausen J., Kroupa P., Baumgardt H., 2009, *MNRAS*, 394, 1529
 de Vries B. L., Min M., Waters L. B. F. M., Blommaert J. A. D. L., Kemper F., 2010, *A&A*, 516, A86+
 Demyk K., et al. 2001, *A&A*, 368, L38
 Dunne L., Eales S., Ivison R., Morgan H., Edmunds M., 2003, *Nature*, 424, 285
 Elvis M., Marengo M., Karovska M., 2002, *ApJ*, 567, L107
 Fox O. D., Chevalier R. A., Dwek E., Skrutskie M. F., Sugerman B. E. K., Leisenring J. M., 2010, *ApJ*
 Gillett F. C., Forrest W. J., Merrill K. M., Soifer B. T., Capps R. W., 1975, *ApJ*, 200, 609
 Hao L., et al. 2005, *ApJ*, 625, L75
 Jaffe W., et al. 2004, *Nature*, 429, 47
 Jäger C., Fabian D., Schrempel F., Dorschner J., Henning T., Wesch W., 2003, *A&A*, 401, 57
 Jäger C., Molster F. J., Dorschner J., Henning T., Mutschke H., Waters L. B. F. M., 1998, *A&A*, 339, 904
 Jones A. P., Tielens A. G. G. M., Hollenbach D. J., 1996, *ApJ*, 469, 740
 Jones A. P., Tielens A. G. G. M., Hollenbach D. J., McKee C. F., 1994, *ApJ*, 433, 797
 Kemper F., Vriend W. J., Tielens A. G. G. M., 2004, *ApJ*, 609, 826
 Kemper F., Vriend W. J., Tielens A. G. G. M., 2005, *ApJ*, 633, 534
 Kemper F., Waters L. B. F. M., de Koter A., Tielens A. G. G. M., 2001, *A&A*, 369, 132
 Kennicutt Jr. R. C., 1998, *ARA&A*, 36, 189
 Kippenhahn R., Weigert A., 1990, *Stellar Structure and Evolution*. *Stellar Structure and Evolution*, XVI, 468 pp. 192 figs.. Springer-Verlag Berlin Heidelberg New York. Also *Astronomy and Astrophysics Library*
 Krause O., Birkmann S. M., Rieke G. H., Lemke D., Klaas U., Hines D. C., Gordon K. D., 2004, *Nature*, 432, 596
 Kroupa P., 2001, *MNRAS*, 322, 231
 Markwick-Kemper F., Gallagher S. C., Hines D. C., Bouwman J., 2007, *ApJ*, 668, L107
 McQuinn K. B. W., et al. 2010, *ApJ*, 724, 49
 Molster F., Kemper C., 2005, *Space Science Reviews*, 119, 3
 Molster F. J., et al. 1999, *A&A*, 350, 163
 Morgan H. L., Dunne L., Eales S. A., Ivison R. J., Edmunds M. G., 2003, *ApJ*, 597, L33
 Rho J., Reach W. T., Tappe A., Hwang U., Slavin J. D., Kozasa T., Dunne L., 2009, *ApJ*, 700, 579
 Salpeter E. E., 1955, *ApJ*, 121, 161
 Siebenmorgen R., Haas M., Krügel E., Schulz B., 2005, *A&A*, 436, L5
 Spoon H. W. W., et al. 2006, *ApJ*, 638, 759
 Sturm E., et al. 2000, *A&A*, 358, 481
 Sugerman B. E. K., et al. 2006, *Science*, 313, 196
 Sylvester R. J., Kemper F., Barlow M. J., de Jong T., Waters L. B. F. M., Tielens A. G. G. M., Omont A., 1999, *A&A*, 352, 587
 Tinsley B. M., 1980, *Fundamentals of Cosmic Physics*, 5, 287
 Verhoelst T., van der Zypen N., Hony S., Decin L., Cami J., Eriksson K., 2009, *A&A*, 498, 127
 Voors R. H. M., Waters L. B. F. M., Morris P. W., Trams N. R., de Koter A., Bouwman J., 1999, *A&A*, 341, L67
 Weedman D. W., Houck J. R., 2008, *ApJ*, 686, 127
 Zhukovska S., Gail H.-P., Trieloff M., 2008, *A&A*, 479, 453